Plant Biotechnology 38, 355–366 (2021)
DOI: 10.5511/plantbiotechnology.21.0730a

Original Paper

Fluorescence from abnormally sterile pollen of the Japanese apricot

Shinnosuke Mori[1,*,a], Shuichi Shimma[2], Hiromi Masuko-Suzuki[3], Masao Watanabe[3], Tetsu Nakanishi[4], Junko Tsukioka[5], Katsumi Goto[5,b], Hiroshi Fukui[6,b], Nobuhiro Hirai[1,b]

[1] Graduate School of Agriculture, Kyoto University, Kyoto, Kyoto 606-8502, Japan; [2] Graduate School of Engineering, Osaka University, Osaka, Osaka 565-0871, Japan; [3] Graduate School of Life Sciences, Tohoku University, Sendai, Miyagi 980-8577, Japan; [4] Graduate School of Agriculture, Kobe University, Kobe, Hyogo 657-8501, Japan; [5] The Garden of Medicinal Plants, Kyoto Pharmaceutical University, Kyoto, Kyoto 601-1405, Japan; [6] Faculty of Agriculture, Kagawa University, Miki, Kagawa 761-0795, Japan
* E-mail: mori.shinnosuke.72x@kyoto-u.jp Tel: +81-45-566-1577

Received June 21, 2021; accepted July 30, 2021 (Edited by Y. Itoh)

Abstract We observed trees of the Japanese apricot, *Prunus mume* 'Nanko' (Rosaceae), bearing two types of flowers: 34% had blue fluorescent pollen under UV irradiation, and 66% had non-fluorescent pollen. The fluorescent pollen grains were abnormally crushed, sterile, and devoid of intine and pollenkitt. The development of microspores within anthers was investigated: in the abnormally developed anthers, tapetal cells were vacuolated at the unicellular microspore stage, and fluorescent pollen was produced. Compounds responsible for the blue fluorescence of pollen were identified as chlorogenic acid and 1-*O*-feruloyl-*β*-D-glucose. The anthers with fluorescent pollen contained 6.7-fold higher and 3.8-fold lower amounts of chlorogenic acid and N^1,N^5,N^{10}-tri-*p*-coumaroylspermidine, respectively, compared to those with non-fluorescent pollen. The tapetal vacuolization, highly accumulated chlorogenic acid, and deficiency of N^1,N^5,N^{10}-tri-*p*-coumaroylspermidine imply that low-temperature stress during the early unicellular microspore stage caused a failure in microsporogenesis. Furthermore, potential effects of the visual difference on the bee behavior were also discussed through the colorimetry. The sterility, likely induced by low-temperature stress, and the preference of honeybees for fluorescence may reduce the pollination efficiency of *P. mume*.

Key words: fluorescence, pollen, pollination, *Prunus mume*, sterility.

Introduction

The Japanese apricot, *Prunus mume* (Rosaceae), is a deciduous tree native to China, and is considered to have been introduced into Japan ca. 2,000 years ago (Hayashi et al. 2008). A wide variety of cultivars are grown for ornamental and commercial purposes, and their fruits are usually consumed in pickles and liqueurs. The annual yield of *P. mume* fruit fluctuated between 5.47 and 7.64 t ha^{-1} in 2007–2016, based on statistics from the Ministry of Agriculture, Forestry and Fisheries of Japan (2018). These yields are one of the poorest levels among major fruit trees in Japan. For example, in the apple tree (*Malus domestica*), the annual yield was17.34–23.06 t ha^{-1} in the same period. The low and fluctuating yield of *P. mume* is considered to be due to the self-incompatibility and male sterility of major cultivars and the occurrence of imperfect flowers (Burgos et al. 2004; Tao et al. 2002; Yaegaki et al. 2003). The imperfect flowers are characterized by pistil abortion. These flowers usually show withered, short, and/or curved pistils, or in serious cases, absence of pistils (Hou et al. 2011; Nakanishi 1982; Sharma and Nayyar 2016; Sun et al. 2016; Zinn et al. 2010). Furthermore, in the flowering period between February and March, temperatures often drop below 15°C, which decreases the foraging activity of pollinating insects. Pollination of *P. mume* is predominantly achieved by the western honeybee, *Apis mellifera* L., introduced

Abbreviations: AUC, area under spectral curve; DAPI, 4′,6-diamidino-2-phenylindole; DW, dry weight; HPLC, high performance liquid chromatography; LC-MS, liquid chromatography-mass spectrometry; MALDI, matrix assisted laser desorption/ionization; NMR, nuclear magnetic resonance; SD, standard deviation; SEM, scanning electron microscopy; TEM, transmission electron microscopy; UPLC, ultra performance liquid chromatography; UV, ultraviolet.

[a] Present address: Faculty of Science and Technology, Keio University, Yokohama, Kanagawa 223-8522, Japan
[b] Deceased

This article can be found at http://www.jspcmb.jp/
Published online September 18, 2021

into orchards, so that the foraging activity of honeybees is critical for ensuring fruit set (Nakanishi and Ichii 1978; Potts et al. 2016). The pollen of *P. mume* is a valuable resource for honeybees in early spring after winter clustering. Information on the floral characteristics of *P. mume* in relation to the foraging activity of honeybees remains limited.

Nakanishi (1982) examined the visual difference in the flowers between male-fertile and -sterile cultivars of *P. mume*, and observed that the anthers of sterile cultivars 'Shirokaga', 'Gyokuei', and 'Gojiro' fluoresce under UV irradiation, while those of fertile cultivars 'Koshusaisho', 'Oshuku', and 'Aogiku' do not. Recently, we have found that the most cultivated male-fertile cultivar 'Nanko' bears two types of flowers on individual trees: flowers with anthers producing pollen that emits blue fluorescence under UV irradiation and those with anthers producing non-fluorescent pollen (Mori et al. 2019). The visual difference may be a consequence of their development and may influence the foraging behavior of honeybees. In this study, we examined the difference in development between the non-fluorescent and fluorescent pollen of *P. mume* 'Nanko' in relation to the foraging behavior of honeybees.

Materials and methods

Plant material

Flowers and buds of the Japanese apricot, *Prunus mume* Siebold & Zucc. 'Nanko' (Rosaceae), were collected at the Garden of Medicinal Plants, Kyoto Pharmaceutical University (Kyoto, Japan) and the experimental farm of Kyoto University (Kyoto, Japan) from February to March 2017.

Photography

Photographs of flowers were taken with an EOS 60D camera (Canon, Tokyo, Japan) equipped with an EF-S60 mm F2.8 MACRO USM lens (Canon). The anthers and pollen were photographed with the EOS 60D camera connected to an SMZ-1500 stereomicroscope (Nikon, Tokyo, Japan) or a BX50 upright light microscope (Olympus, Tokyo, Japan). Fluorescent lamps HGX FHF32EX (32 W; NEC lighting, Tokyo, Japan) were used for white light illumination, and two Handy UV lamps LUV-16 (365 nm, 16 W; ASONE, Osaka, Japan) for UV illumination.

Reagents

9-Aminoacridine was purchased from Tokyo Chemical Industry (Tokyo, Japan). Other reagents were purchased from Wako Pure Chemical Industries, Ltd. (Osaka, Japan). Wakogel® C-200 silica gel (Wako Pure Chemical Industries, Ltd.) was used for silica gel column chromatography. Ultrapure water was obtained by a GenPure UV-TOC xCAD Plus water purification system (Thermo Fisher Scientific, MA, USA). All reagents were of analytical grade.

Pollen germination test

Anthers were incubated for dehiscence at 20°C for 10 h in an IC800 incubator (Yamato Scientific, Osaka, Japan). From the dehisced anthers, non-fluorescent and fluorescent pollen were collected under UV illumination. The two types of pollen grains were cultivated separately on medium containing 1% agar ($w v^{-1}$), 15% sucrose ($w v^{-1}$), and 0.01% boric acid ($w v^{-1}$) for 12 h in the dark. Temperature and humidity were maintained at 20°C and 85%, respectively, during the tests. The tests were replicated three times for both types of pollen, and germination rates are presented as mean±SD The non-fluorescent and fluorescent pollen grains were stained for 5 min with Lugol's solution (Johansen 1940).

Electron microscopy

For SEM, dehisced anthers containing pollen were collected from fresh opened flowers. The anthers were soaked in FAA fixative (63% EtOH, 5% AcOH, and 5% HCHO) at 4°C overnight. The fixed anthers were dehydrated in a graded ethanol series and in *t*-butyl alcohol, and then freeze-dried at −20°C. The dried anthers were mounted on stages and coated with platinum in an ion coater IB-3 (Eiko Engineering, Tokyo, Japan). The anthers were observed by an SEM S-4700 (Hitachi, Tokyo, Japan) at an acceleration voltage of 5.0 kV.

For TEM, dehisced anthers were soaked in half Karnovsky's fixative for 30 h. The fixed anthers were rinsed with 0.1 M phosphate buffer, followed by post-fixation with 1% osmium tetroxide at 4°C overnight. The anthers were dehydrated in a graded ethanol series and embedded in Plain Resin (Nisshin EM, Tokyo, Japan) at 70°C for 5 days. Ultrathin sections were prepared by an EM UC6 ultramicrotome (Leica, Heidelberg, Germany) using a diamond knife. The sections were stained with 1% uranyl acetate and then with lead citrate. The prepared sections were placed on copper grids and observed with a TEM H-7650 (Hitachi, Tokyo, Japan). Images were captured with an AMT XR-41C CCD camera system (Advanced Microscopy Techniques, MA, USA).

Cytohistological analyses

The floral buds and opened flowers were soaked in FAA fixative at 4°C overnight. Tissue fixation and paraffin embedding were performed with a LabPulse H2850 microwave processor (Energy Beam Sciences, CT, USA), according to Osaka et al. (2013), with minor modifications. All samples were embedded in Paraplast X-TRA paraffin (Fisher Scientific, Hampton, NH, USA). Paraffin blocks were stored at 4°C until use. The samples were cut into 10 μm-thick sections using a microtome RV240 (Yamato Koki, Saitama, Japan). Sections were placed on glass slides (Matsunami Glass, Osaka, Japan) and baked at 50°C overnight. Paraffin was removed with Histo-Clear II (National Diagnostics, GA, USA). After rehydration by an ethanol series, the sections were stained with periodic acid-Schiff (PAS) stain kit (Muto Pure Chemicals, Tokyo, Japan). The stained sections were placed in Multimount 480 mounting medium (Matsunami Glass). The prepared sections were stained with DAPI

(4′,6-diamidino-2-phenylindole) staining solution (Watanabe et al. 1991) and then mounted in 70% glycerol medium. All section images were obtained with a SteREO Discovery V20 stereomicroscope (Carl Zeiss, Jena, Germany).

Colorimetry

Diffuse reflectance spectra of the intact anthers and petals were measured from 350 nm to 700 nm, using a V-670 spectrometer (Jasco, Tokyo, Japan) equipped with an ISN-723 integrating sphere unit (Jasco). Dehisced anthers with pollen and fresh petals were used for the measurements. The spectra were measured in an FPA-810 powder sample cell (Jasco). Spectralon (Labsphere, NH, USA) was used as a white standard for calibration. Data were processed using Spectra Manager version 2.10.01 (Jasco).

Color loci of the anthers with pollen in the color hexagon space (Chittka 1992) were calculated in R (R Core Team 2016) using the package 'pavo' version 1.3.2 (Maia et al. 2013) with reflectance spectra from 350 nm to 650 nm, which is the spectral sensitivity of honeybees, *Apis mellifera* L. (Peitsch et al. 1992). The irradiance spectrum of the International Commission on Illumination CIE D65 was applied as a model of daylight irradiance. The reflectance of petals was assumed to be the background of anthers. The hexagon was divided into six categories (UV, UV-blue, blue, blue-green, green, and UV-green), which refer to the stimulation of honeybee photoreceptors. Chromatic contrasts were evaluated by the Euclidian distances (hex units) (Chittka 1992).

TLC, HPLC, LC-MS, and NMR analyses

TLC Silica gel 60 F254 Alminum sheets (Merck, Darmstadt, Germany) were used for TLC analyses. A mixture of MeOH–$CHCl_3$–AcOH in the ratio of 15 : 5 : 1 was used as the developing solvent.

HPLC was performed on an L-7100 series system (Hitachi, Tokyo, Japan) consisting of an L-7100 pump (Hitachi) and an L-7400 detector (Hitachi) with the following conditions: column, a YMC-Pack ODS-AQ (6.0 mm inner diameter ×100 mm; YMC, Kyoto, Japan); eluent, H_2O–MeOH–AcOH; flow rate, 1.0 ml min^{-1}; and detection, UV 254 nm.

LC-MS analyses were performed on an Acquity UPLC system H class and a Xevo G2-S QTof MS (Waters, MA, USA) with an Acquity UPLC BEH C18 column (polar size, 1.7 μm, 2.1 mm inner diameter ×100 mm; Waters). The analyses were conducted with the following conditions: eluent, 22% MeCN containing 0.1% HCO_2H for 10 min and 50% MeCN containing 0.1% HCO_2H for 10–15 min; flow rate, 0.3 ml min^{-1}; detection, UV 254 nm. MS was operated with electron spray ionization in positive mode under the following parameters: column oven, 35°C; capillary voltage, 3.0 kV; cone voltage, 40 V; source temperature, 150°C; desolvation temperature, 500°C; cone gas, 50 l h^{-1}; desolvation gas, 800 l h^{-1}. Data processing was performed using MassLynx version 4.1 (Waters).

^{1}HNMR spectra were measured in methanol-d_4 (Sigma-Aldrich, MO, USA) at 25°C with an AVANCE III 400 spectrometer (Bruker, Rheinstetten, Germany). Data processing was performed using TopSpin version 3.0 (Bruker).

Isolation and quantification of compounds 1–4

Non-fluorescent anthers with pollen (1.4 g fresh weight) were soaked in 30 ml of MeOH at 4°C for 5 days. The extract was filtered and concentrated in vacuo to give an oily residue (136 mg). The residue was partitioned with EtOAc and H_2O three times. The material from the organic layer was applied to a silica gel column (10 mm inner diameter ×70 mm) with eluent of $CHCl_3$–MeOH (5 ml for each fraction). The material eluted with 30% MeOH was concentrated to give compound **1**. The material eluted with 20% MeOH was subjected to preparative HPLC (eluent: 0.1% AcOH in 40% MeOH) to give two fractions at *t*R 0–11.4 min (fraction 1) and 14.2 min (fraction 2). Fraction 1 was subjected to preparative HPLC (eluent: 0.1% AcOH in 20% MeOH), and the materials eluted at *t*R 17.3 min and 20.1 min were collected and concentrated to give compounds **2** (0.2 mg) and **3** (trace), respectively. Fraction 2 was concentrated to give compound **4** (1 mg).

Quantification was performed with HPLC. The amounts of **1**–**4** in the extracts were calculated with a calibration curve between the weight and peak area, using a known solution of each isolated compound as the standard. The amounts of the mixtures of **6**–**8** and **9**–**11**, and of **12** were quantified with isolated **5** as the standard on an assumption of the same molar extinction coefficient of **5**–**12**.

UV/Visible absorption and fluorescence spectral analyses

UV/Vis spectra of MeOH solutions were measured with a UV-1800 spectrometer (Shimadzu, Kyoto, Japan). Fluorescence spectra were measured with an FP-8300 spectrofluorometer (Jasco, Tokyo, Japan). An FUV-803 absorbance measurement cell block (Jasco) was used for solutions, and an FPA-810 powder sample cell block for the intact dehisced anthers with pollen. The absorption spectra were measured from 200 nm to 550 nm, and the excitation and emission spectra of the anthers with pollen from 300 nm to 600 nm. The samples of anthers with pollen were randomly divided into three sets. The spectra with each set were averaged. The fluorescence spectral data were processed with Spectra Manager version 2.10.01 (Jasco). The area under spectral curve of emission (AUC_{Em}) of anthers and pollen was integrated.

MALDI-MS/MS imaging analyses

For sample treatment, the anthers with non-fluorescent pollen and those with fluorescent pollen were collected individually and embedded in 4% carboxymethyl cellulose (CMC; Leica, Wetzlar, Germany). Embedding was performed in a base mold (7 mm×7 mm×5 mm) (FALMA, Tokyo, Japan). The anthers were slowly mixed to disperse in the CMC. After dispersion, the molds were stored in a freezer at −80°C until completely frozen. Before cutting tissue sections, the CMC blocks with anthers were put in a cryomicrotome CM1950 (Leica) at

−20°C for 10 min. The blocks were put on the tissue-holder, fixed with optimum cutting temperature polymer (Leica), and cut at 10 μm-thickness. The tissue sections were collected onto cryofilm (Leica). The obtained section on the film was mounted onto indium-tin-oxide-coated glass slides (100 Ω m^{-2} without anti-peeling coating; Matsunami Glass, Osaka, Japan) via double-sided adhesive conductive tape (3M, MN, US). The glass slides were dried at room temperature in 50 ml conical tubes with silica gel.

9-Aminoacridine was applied to the tissue sections by the recrystallization method, combining sublimation and exposure to 5% methanol vapor. For sublimation, 9-aminoacridine was heated at 220°C and deposited on the surface of the tissue sections in iMLayer (Shimadzu, Kyoto, Japan) until the thickness of the matrix reached 0.5 μm. After covering the sections with a 9-aminoacridine layer, 5% methanol with H_2O vapor was provided for 3 s, and they were then dried at room temperature.

Imaging mass spectrometry was performed with an iMScope TRIO (Shimadzu, Kyoto, Japan). Both optical images and ion distribution could be obtained within the same instrument under atmospheric pressure. A Nd:YAG laser (λ 355 nm, 1 kHz) was used as the matrix-assisted laser desorption/ionization (MALDI) laser source, and laser irradiation was repeated 80 times on each data point with a laser power of 45.0 (arbitrary unit in iMScope TRIO). Negative and positive ion modes were used to detect **2** and **5**–**12**, respectively. To enhance the specificity, MS/MS imaging was performed using the transition m/z 353.08>191.04 for **2** and m/z 584.28>420.22 for **5**–**12**. Voltages of the sample stage and detector were 3.0 kV and 2.1 kV, respectively. Imaging data was reconstructed using BioMap 3.8 (Mass Spectrometry Imaging Society, https://ms-imaging.org/wp/).

Results

Morphology and viability of pollen grains

The two types of flowers of *Prunus mume* 'Nanko' are shown in Figure 1A, that is flowers with anthers bearing pollen grains that emit blue fluorescence under UV irradiation and those that do not. Approximately 34±4% of flowers on each tree bore fluorescent pollen at the time of blooming (n=3). Under white light, the non-fluorescent pollen appeared yellow (Figure 1B), whereas the fluorescent pollen appeared white (Figure 1C). The anthers with white pollen had relatively lighter yellow anther walls. The yellow pollen and the anther walls did not emit fluorescence. The color difference between the two types of anthers is discussed in section *Colorimetry of the anthers with pollen grains*. The anthers bearing fluorescent pollen were slightly smaller than those with non-fluorescent pollen (Figure 1B, C). There appeared to be no difference between the two types of flowers in other floral structures such as the pistil, petal, and sepal.

SEM showed that the non-fluorescent pollen grains

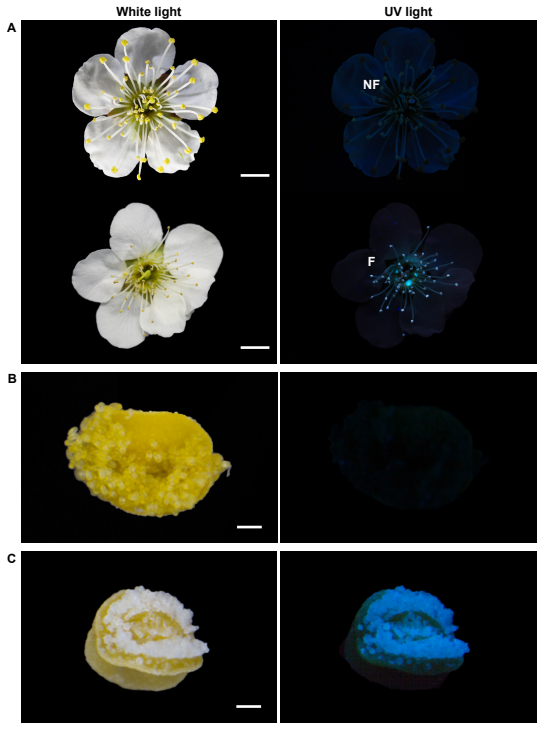

Figure 1. Photographs of the two types of flowers of *Prunus mume* 'Nanko' under white light (left) and UV light (365 nm; right). (A) Flowers with anthers bearing non-fluorescent pollen (NF; upper) and those bearing fluorescent pollen (F; lower). Dehisced anthers with (B) non-fluorescent and (C) fluorescent pollen. Scale bars: (A) 1 cm; (B, C) 100 μm.

were elliptical and triaperturate with the germinal furrow extending almost the full length of the grains (Figure 2A, B). On the other hand, the fluorescent pollen grains were abnormally collapsed and firmly fixed to the anther wall. The sexine of the non-fluorescent pollen grains had a striate ornamentation pattern with perforated tectum (Figure 2C). Although the fluorescent pollen grains showed a similar pattern to the non-fluorescent ones, no tectal perforations were observed. Cross-sectional ultrastructure of the pollen grains was examined by TEM, which confirmed plasmolysis of the fluorescent pollen (Figure 2D). The non-fluorescent pollen showed a pollen wall consisting of intine, continuous thin endexine, foot layer, columella, tectum, and pollenkitt filling the sculptured cavities of exine (Figure 2E; Punt et al. 2007). The striate ornamentation pattern and exine stratification structure of the non-fluorescent pollen are mostly consistent with other Rosaceae species (Song et al. 2016, 2017). The fluorescent pollen grains exhibited densely and nonuniformly arranged exine and defective intine, and lacked pollenkitt.

The non-fluorescent pollen accumulated starch granules, as confirmed by staining with Lugol's solution (Figure 3A). However, the fluorescent pollen grains were almost devoid of starch granules. The germination rate of the non-fluorescent pollen was 60.5±4.8% in vitro,

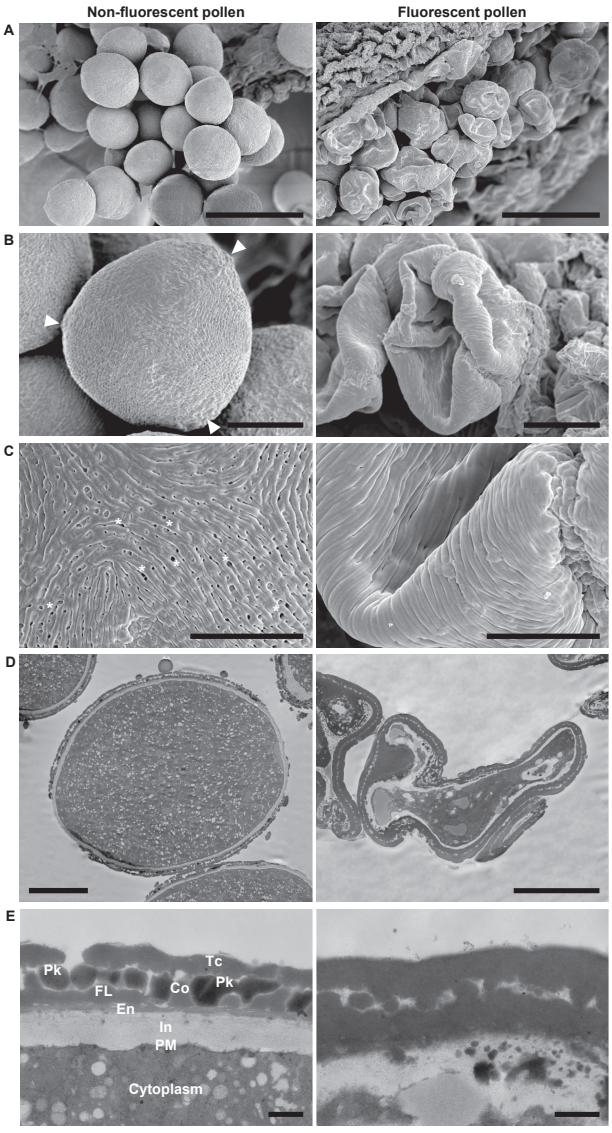

Figure 2. Electron microscopic images of non-fluorescent pollen (left) and fluorescent pollen (right) at the bicellular pollen stage. SEM micrographs of (A) pollen, (B) whole grains, and (C) magnified views. Arrowheads and asterisks indicate the tectal perforations and apertures, respectively. TEM micrographs of sections of pollen: (D) whole grains and (E) details of the pollen wall. Scale bars: (A) 50 μm, (B) 10 μm, (C) 5 μm, (D) 10 μm, (E) 500 nm. In, intine; PM, plasma membrane; En, endexine; FL, foot layer; Co, collumera; Tc, tectum; Pk, pollenkitt.

whereas that of the fluorescent pollen was 0% (Figure 3B).

Pollen development within anthers

Development of anthers and pollen was investigated using floral buds at different stages to determine how the fluorescent pollen grains developed. Pollen development was classified into three stages according to the number of DAPI-stained pollen nuclei: unicellular microspore stage, bicellular pollen stage, and interphase containing both unicellular and bicellular pollen (Figure 4). At the unicellular microspore stage, all anthers contained microspores surrounded by tapetum, middle layer,

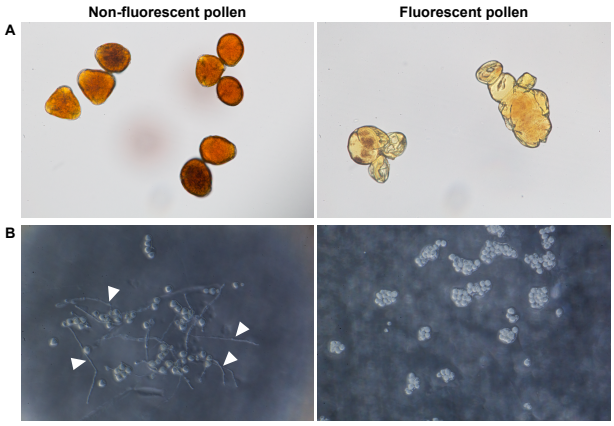

Figure 3. Viabilities of non-fluorescent pollen (left) and fluorescent pollen (right). (A) Pollen after 2 min cultivation in Lugol's solution. (B) Pollen after 12 h cultivation on 1% agar medium with 15% sucrose and 0.01% boric acid. Arrowheads indicate pollen tubes.

endothecium, and epidermis (Figure 4D, M; Sanders et al. 1999). In the normally developing anthers, a tapetal programmed cell death was initiated between the unicellular microspore stage and interphase (Figure 4D, E; Quilichini et al. 2015), and degeneration of the tapetum was complete by the bicellular pollen stage (Figure 4F).

Several anthers displayed abnormally vacuolated tapetal cells at the unicellular microspore stage and interphase (Figure 4M, N). At later stages, the vacuolated tapetum disappeared, and all pollen had collapsed (Figure 4O). Although the anthers, such as in Figure 4O, appeared to be at the bicellular pollen stage according to the degenerated tapetum, nuclei were not detected in the pollen.

Under UV 365 nm irradiation, both the normally and abnormally developed microspores emitted bright blue fluorescence at the unicellular microspore stage (Figure 4G, P). While the fluorescence of the normally developing microspores almost disappeared at interphase (Figure 4H), that of the abnormally developing microspores was still present at the bicellular pollen stage (Figure 4P–R).

Colorimetry of the anthers with pollen grains

The visible spectrum of honeybee vision, *Apis mellifera* L., ranges from approximately 300 nm to 650 nm based on trichromatic vision, with the maxima of sensitivities at UV (344 nm), blue (436 nm), and green (544 nm), whereas that of humans ranges from approximately 400 nm to 700 nm (Bowmaker and Dartnall 1980; Peitsch et al. 1992). The color of petals and anthers with pollen from the two types of flowers was analyzed to examine whether honeybees can distinguish between them by reflectance. The diffuse reflectance spectrum of the anthers with fluorescent pollen showed 1.0–9.3% higher reflectance than that of the anthers with non-fluorescent

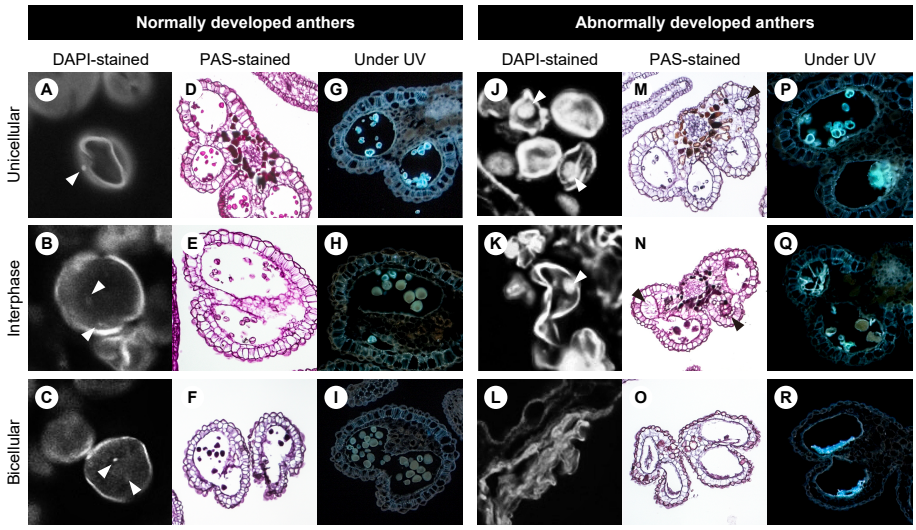

Figure 4. Sections of normally developed anthers with pollen (A–I) and abnormally developed anthers (J–R) at the unicellular microspore stage (A, D, G, J, M, P), interphase (B, E, H, K, N, Q), and bicellular pollen stage (C, F, I, L, O, R). Arrowheads indicate nuclei in (A–C, J, K) and vacuolated tapetum in (M, N).

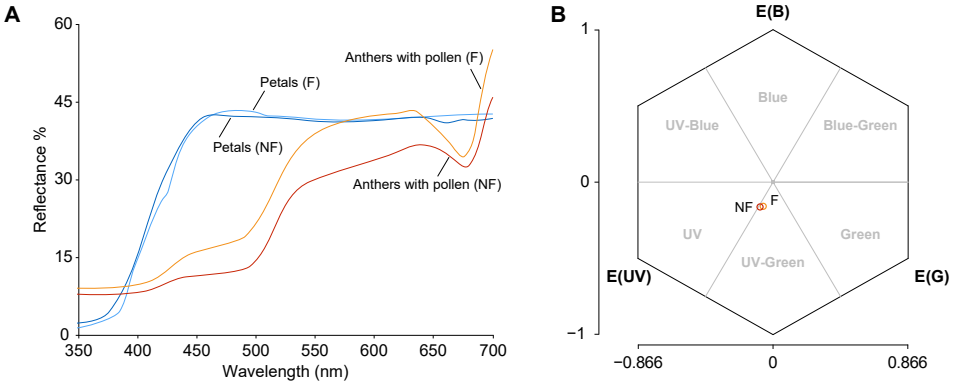

Figure 5. Reflectance characteristics of anthers with pollen and petals. (A) Diffuse reflectance spectra of anthers with pollen (red) and petals (blue) from flowers bearing non-fluorescent pollen (NF), and of anthers with pollen (orange) and petals (light blue) from flowers bearing fluorescent pollen (F). (B) Color loci of anthers with non-fluorescent pollen (red) and anthers with fluorescent pollen (orange) plotted in a bee color hexagon (Chittka 1992). E (UV), E (B), E (G): excitation of the UV-, blue-, and green-sensitive photoreceptors, respectively.

pollen across the range of 350 nm to 700 nm (Figure 5A). The petals of both types of flowers displayed almost the same reflectance spectra; therefore, the averaged reflectance spectrum of the petals was applied as a background of the anthers for the calculations.

The color loci of the anthers with pollen in a color hexagon space were calculated in relation to the spectral sensitivity of the honeybee photoreceptors (Figure 5B; Chittka 1992; Peitsch et al. 1992). The color loci of both types of anthers with pollen were classified as bee-UV-Green. The color distance from the center, representing the background petal, to the anthers with non-fluorescent pollen was 0.236 hex units and that to the anthers with fluorescent pollen was 0.218 hex units. The pairwise distance between the color loci of the two types of anthers with pollen was 0.024 hex units.

Because the diffuse reflectance spectra do not include fluoresced photons, the fluorescence characteristics of the anthers with pollen were determined with the fluorescence spectra (Figure 6A), and their intensities were evaluated by areas under the curves of emission spectra (AUC_{Em}; Figure 6B). The anthers with non-fluorescent pollen displayed excitation maxima (λ_{Ex}) at 324 nm and emission maxima (λ_{Em}) at 439 nm, and those with fluorescent pollen displayed λ_{Ex} and λ_{Em} at 340 nm and 444 nm, respectively. The AUC_{Em} of the anthers with fluorescent pollen was significantly higher than those with non-fluorescent pollen (6.3-fold, t (4)=21.59, $p<0.001$; Figure 6B).

Isolation and identification of major constituents from anthers and pollen grains

The chemical constituents of the non-fluorescent and fluorescent anthers were analyzed by HPLC. The extracts from the anthers with non-fluorescent pollen yielded three fluorescent compounds (**1**–**3**); one yellow

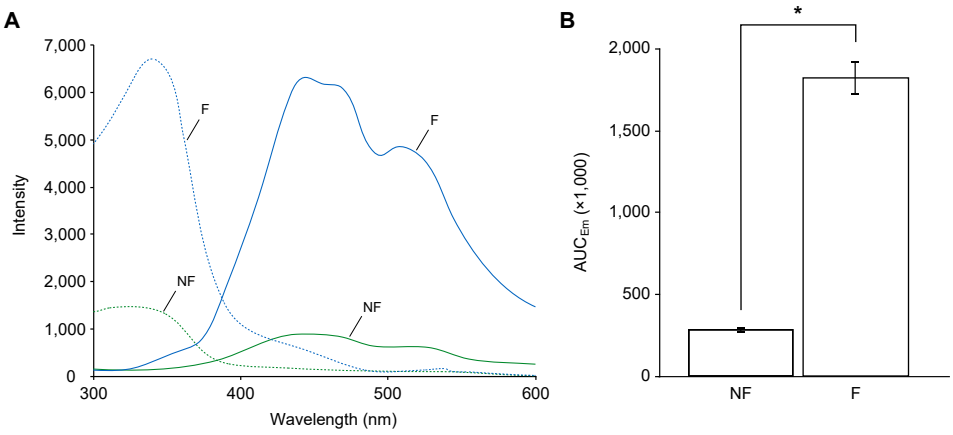

Figure 6. Fluorescence characteristics of anthers with pollen and petals. (A) Excitation spectra (dashed lines) and emission spectra (Em; solid lines) of anthers with non-fluorescent pollen (green) and those with fluorescent pollen (blue). (B) AUC_{Em} of the two types of anthers with pollen. NF, anther with non-fluorescent pollen; F, anther with fluorescent pollen. AUC_{Em} represents the intensity of emission between 350 and 600 nm. Error bars indicate SD. * $p<0.001$ determined by Student's *t*-test.

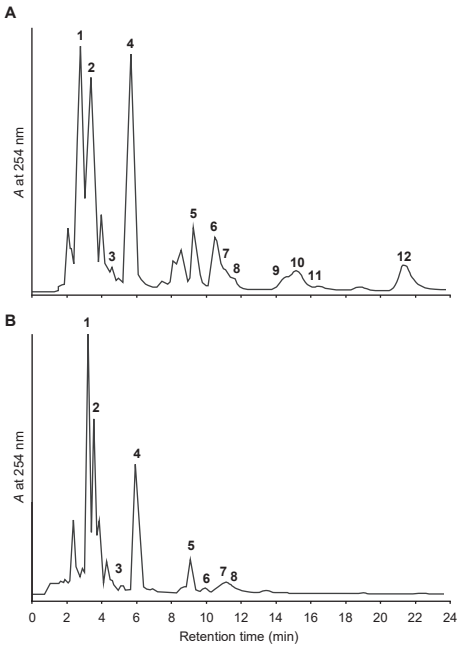

Figure 7. HPLC chromatograms of an extract from anthers with pollen. (A) Extract from anthers with non-fluorescent pollen and (B) anthers with fluorescent pollen. Operating conditions: column, ODS; solvent, 0.1% AcOH in 39% MeOH (1 ml min^{-1}); detection, UV 254 nm.

pigment (**4**); and eight non-fluorescent UV-absorbing compounds (**5**–**12**) as major constituents (Figure 7A). We have previously reported the identification of **1** and **5**–**12** as (*E*)-chlorogenic acid (**1**), N^1,N^5,N^{10}-tri-*p*-(*ZZZ*)-coumaroylspermidine (**5**), and its (*ZEZ*)- (**6**), (*EZZ*)- (**7**), (*ZZE*)- (**8**), (*EZE*)- (**9**), (*ZEE*)- (**10**), (*EEZ*)- (**11**), and (*EEE*)-isomers (**12**) (Mori et al. 2019). In the extract from the anthers with fluorescent pollen, **1**–**3**, **5**, and a limited amount of **6**–**8** were detected, but **9**–**12** were not (Figure 7B). Compounds **2**–**4** were isolated from the extract of the anthers with non-fluorescent pollen, while monitoring the blue fluorescence and yellow coloration on TLC; they were identified as 1-*O*-(*E*)-feruloyl-*β*-D-glucose (**2**; Birkofer et al. 1961; Bokern et al. 1987) and its (*Z*)-isomer (**3**; Hixson et al. 2016), and quercetin 3-*O*-*β*-D-glucoside (**4**; Bennini et al. 1992; Perkin, 1909), based on its ^{1}H NMR and LC-MS spectral data.

Amounts of **1**–**12** in the anthers with pollen are summarized in Table 1. The amount of **1** was 3.2 mg g^{-1} DW in the anthers with non-fluorescent pollen, whereas it was significantly higher in the anthers with fluorescent pollen (21.6 mg g^{-1} DW; 6.8-fold). The amount of **4** was significantly higher in the anthers with non-fluorescent pollen, compared to the anthers with fluorescent pollen (17.1 vs 11.2 mg g^{-1} DW; 1.5-fold). In contrast, the total amount of *E*/*Z* isomers **5**–**12** was higher in the anthers with non-fluorescent pollen than with fluorescent pollen (12.2 vs 3.2 mg g^{-1} DW; 3.8-fold). There was no significant difference in the total amount of *E*/*Z* isomers **2** and **3** between the two types of anthers with pollen (2.1 vs 1.6 mg g^{-1} DW).

Fluorescence and UV/Vis absorption spectral profiles of compounds 1–12

The excitation and emission spectra of **1**–**3** and absorption spectra of **4** and **5** as a major isomer of N^1,N^5,N^{10}-tri-*p*-coumaroylspermidine are summarized in Figure 8. Fluorescence spectra of **1**–**3** had the following λ_{Ex} and λ_{Em}: 383 nm and 453 nm (**1**); 355 nm and 433 nm (**2**); and 339 nm and 431 nm (**3**), respectively (Figure 8; Mori et al. 2018). The UV/Vis absorption spectrum of **4** had an absorption maximum (λ_{Abs}) at 358 nm (Figure 8). The absorption spectra of **5**, mixtures of **6**–**8** (**6**:**7**:**8**=47:26:27) and **9**–**11** (**9**:**10**:**11**=59:12:29), and **12** had λ_{Abs} at 274 nm, 286 nm, 293 nm, and 310 nm, respectively (Mori et al. 2019).

Distribution of 1 and 5–12 in anthers and pollen

The amounts of **1** and **5**–**12** were significantly different

Table 1. Amounts of compounds **1**–**12** in the anthers with pollen.

Compounds	Amount (mg g^{-1} DW)		t (4), p*
	NF	F	
Chlorogenic acid (**1**)	3.2±0.1	21.6±0.7	20.00, <0.01
1-*O*-(*E*)-Feruloyl-*β*-D-glucose (**2**)	2.0±0.2	1.3±0.3	
1-*O*-(*Z*)-Feruloyl-*β*-D-glucose (**3**)	0.1±0.0	0.3±0.0	
Total amount of **2**+**3**	2.1±0.2	1.6±0.2	1.60, 0.18
Quercetin 3-*O*-*β*-D-glucoside (**4**)	17.1±0.5	11.2±0.2	8.91, <0.01
N^1,N^5,N^{10}-Tri-*p*-(*ZZZ*)-coumaroylspermidine (**5**)	4.2±0.3	3.0±0.2	
(*ZEZ*)-isomer (**6**)	3.2±0.2	0.2±0.1	
(*EZZ*)-isomer (**7**)			
(*ZZE*)-isomer (**8**)			
(*EZE*)-isomer (**9**)	1.4±0.1	ND	
(*ZEE*)-isomer (**10**)			
(*EEZ*)-isomer (**11**)			
(*EEE*)-isomer (**12**)	3.4±0.1	ND	
Total amount of **5**–**12**	12.2±0.5	3.2±0.4	14.47, <0.01

Values represents means±SD from three replications. NF, anthers with non-fluorescent pollen; F, anthers with fluorescent pollen; ND, not detected. * Student's *t*-test.

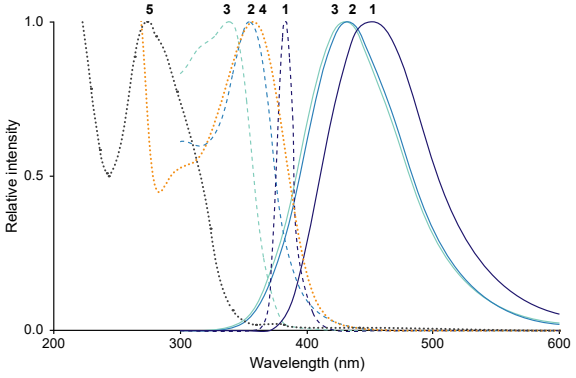

Figure 8. Spectral characteristics of compounds **1**–**5**. Solid line, emission spectra of **1**–**3**; dashed line, excitation spectra of **1**–**3**; dotted line, UV/Vis absorption spectrum of **4** and **5**.

between the two types of anthers with pollen (Table 1). MALDI-MS/MS imaging analyses were performed on tissue to examine the distributions of **1** and **5**–**12** at the bicellular pollen stage. Compound **1** was detected by a fragment ion at *m*/*z* 191.04, corresponding to [M−H−caffeoyl]$^-$ (Figure 9A). The peak intensity of **1** in MS imaging was approximately 3.3-fold higher in the anthers with fluorescent pollen compared to those with non-fluorescent pollen. In the anthers with fluorescent pollen, **1** was distributed throughout the entire anther and pollen, with the highest concentrations in the degraded tapetum, crushed pollen, and epidermis (Figure 9B).

Compounds **5**–**12** (isomers not distinguished) were detected by a fragment ion at *m*/*z* 420.22, corresponding to [M+H−H_2O−coumaroyl]$^+$ (Figure 9C). The peak intensity of **5**–**12** in MS imaging was approximately 14.3-fold higher in the anthers with non-fluorescent pollen compared to the anthers with fluorescent pollen. Compounds **5**–**12** were distributed evenly across the anther and non-fluorescent pollen grains (Figure 9D), with the highest abundance in the pollen. Only a limited amount of **5**–**12** was detected in the anthers with fluorescent pollen.

Discussion

The pollen germination test showed that the fluorescent pollen grains were completely sterile (Figure 3). The occurrence of sterile fluorescent pollen in 34±4% of the flowers on individual trees indicates that these flowers underwent abnormal development. The sterile pollen was abnormally collapsed and devoid of pollenkitt and defective in intine formation (Figure 2). Intine development begins at the unicellular microspore stage, and pollenkitt is provided through tapetal programmed cell death at the bicellular pollen stage (Carrizo García et al. 2017; Sanders et al. 1999). In the abnormally developed anthers, tapetal cells were vacuolated at the unicellular microspore stage and filled the anther locule. The absence of pollenkitt and intine and the vacuolated tapetum suggest a failure in development of the anther and pollen at the early unicellular microspore stage (Figure 4D). Male reproductive development is the stage that is most sensitive to various environmental stresses. Similar tapetal vacuolation has been observed in cold-stressed rice anthers (Mamun et al. 2006, 2010; Oda et al. 2010). In fact, an exposure to cold temperature of flower buds of *P. mume* 'Nanko', the male sterile phenotype was observed (unpublished data).

The anthers with sterile pollen contained a significantly higher amount of fluorescent compound **1**, compared to those with fertile pollen. Phenylpropanoids, including **1**, are induced in response to environmental stresses, including low-temperature (Dixon and Paiva 1995; Koeppe et al. 1970). The tapetal vacuolation at the unicellular microspore stage and the accumulation of stress-induced **1** suggest that low-temperature stress during the early unicellular microspore stage caused

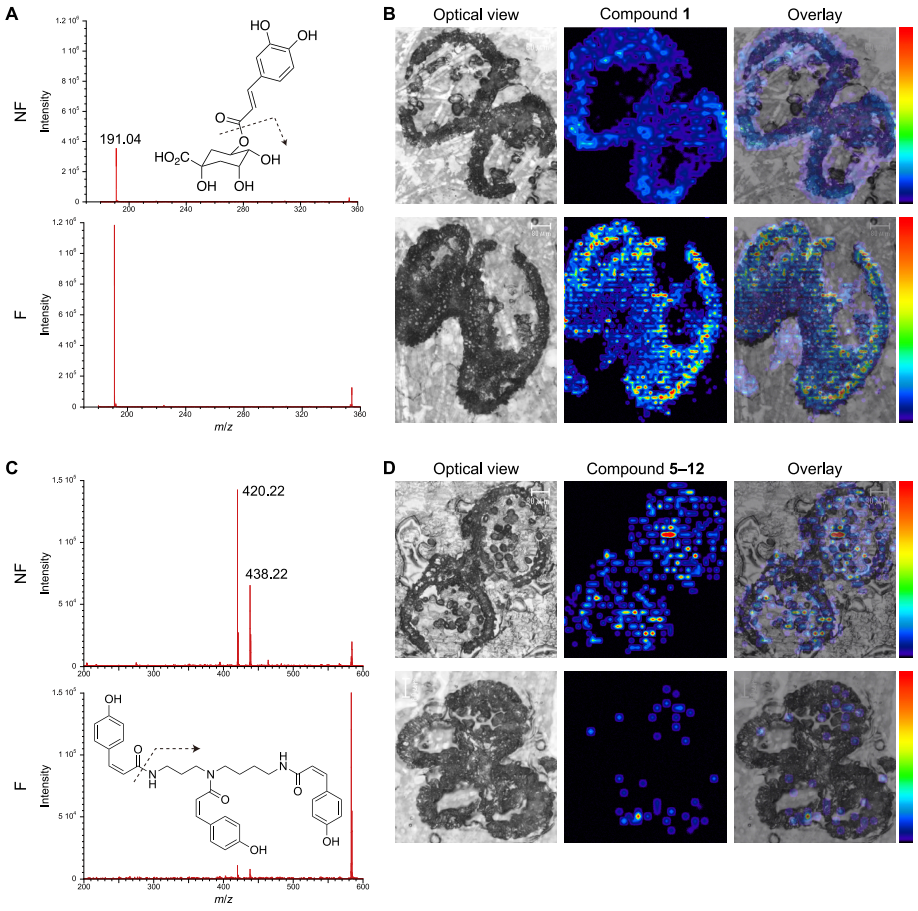

Figure 9. Distributions of compounds **1** and **5**–**12** in anthers and pollen at the bicellular pollen stage. (A) MS chromatograms and (B) distributions of **1** (*m*/*z* 191.04) in anthers with non-fluorescent pollen (NF; upper) and anthers with fluorescent pollen (F; lower), and (C, D) distributions of **5**–**12** (*m*/*z* 420.22; isomers not distinguished).

the abortion of pollen development. MALDI-MS/MS imaging confirmed that a substantial amount of **1** is present on the surface of sterile pollen grains (Figure 9B). Compound **1** may have accumulated in the abnormally vacuolated tapetum and then been deposited onto the surface of sterile pollen by tapetal degradation. The accumulation of compound **1** was also detected in the anther epidermis, but the relationship between this and male infertility is not clear. Compound **1** was distributed throughout even in the anther with sterile pollen, implying some functions in normal development as well.

N^1,N^5,N^{10}-Tri-*p*-coumaroylspermidine isomers have been isolated from the flowers and anthers of many plant species (Bokern et al. 1995; Jiang et al. 2008; Mori et al. 2019; Sobolev et al. 2008; Werner et al. 1995; Zhao et al. 2010). Hydroxycinnamic acid amide (HCAA) derivatives, including **5**–**12**, constitute a group of plant secondary metabolites derived from hydroxycinnamic acid conjugated with polyamines (i.e., putrescine, spermidine, and spermine). HCAAs have been proposed to be involved in polyamine homeostasis and phenolic metabolism (Matsuno et al. 2009; Vogt 2010). Polyamines are essential for growth and survival due to their diverse physiological functions in organogenesis, embryogenesis, floral initiation, and development responses (Alcázar et al. 2010; Martin-Tanguy 2001; Moschou et al. 2012). Crosstalk among polyamines and plant hormones in regulating plant growth and abiotic stress responses has also been elucidated (Anwar et al. 2015; Bassard et al. 2010; Bitrián et al. 2012; Morant et al. 2007; Wimalasekera et al. 2011). Polyamines can be oxidized by polyamine oxidase to generate H_2O_2, which plays roles in defense reactions against abiotic/biotic stress and via H_2O_2 signaling (Liu et al. 2014; Yu et al. 2019). In *P. mume* studied here, the defense reaction against severe low-temperature stress may have been inadequate due to a deficiency in substrates for polyamine oxidase.

MALDI-MS/MS imaging of anthers with non-fluorescent pollen showed that **5**–**12** were distributed across the entire anther and pollen, with the highest amount in the pollen (Figure 9D). This indicates that the pollenkitt of non-fluorescent pollen contains **5**–**12**, as previously found in *Arabidopsis thaliana* (Brassicaceae; Grienenberger et al. 2009) and apple, *Malus domestica* (Rosaceae; Elejalde-Palmett et al. 2015). Spermidine hydroxycinnamoyltransferase

(SHT) catalyzes the conjugation of spermidine to hydroxycinnamoyl-CoA (Elejalde-Palmett et al. 2015; Grienenberger et al. 2009). The *sht* knockout mutant displays an abnormally crushed pollen grain phenotype, indicating hydroxycinnamoylspermidine derivatives are components of sporopollenin (Elejalde-Palmett et al. 2015; Grienenberger et al. 2009). The deficiency of **5**–**12** in the anthers with fluorescent pollen is consistent with a morphological abnormality of exine and suggests that the flowers were exposed to stresses.

Pollenkitt of entomophilous plants typically contains pigments, such as flavonoids and carotenoids (Ferreres et al. 1989; Jiang et al. 2013), that are extractable from the underlying exine with methanol (Mori et al. 2018, 2019). After extraction with methanol, the fertile *P. mume* pollen grains became colorless and exhibited blue fluorescence. Furthermore, in the normally developed anthers, the fluorescence of microspores disappeared as the pollenkitt was deposited on the exine (Figure 4G, H). These findings indicate that the absence of pollenkitt is responsible for the fluorescence and lack of color of sterile pollen. Ferulic acid has been demonstrated to be a precursor of sporopollenin (Rozema et al. 2001; Xu et al. 2017), although the chemical structure of sporopollenin has not been elucidated (Mackenzie et al. 2015; Quilichini et al. 2015). The remnant fluorescence after extraction may be emitted from fluorophores such as caffeoyl and feruloyl moieties embedded in sporopollenin. The UV-absorbing compounds **4**–**12** in the pollenkitt would prevent UV light from reaching the underlying exine; thus, the pollenkitt-covered fertile pollen did not display fluorescence. The anthers with fertile pollen contained relatively small amounts of fluorescent compounds **1**–**3**. As the absorption spectra of **4**–**12** partially overlap with the excitation and emission spectra of **1**–**3** (Figure 8), the high amounts of **4**–**12** may quench the fluorescence of **1**–**3** through the primary and secondary inner-filter effects (Parker and Rees 1962). The emission spectra of **1**–**3** corresponded well with that of the anthers with fluorescent pollen, suggesting that the fluorescence of sterile pollen is derived from these compounds.

Bees can discriminate two colors when their color distance is >0.1 hex units (Chittka et al. 1993), as testified with behavioral tests with several Hymenoptera (Chittka et al. 1992). The color contrast between the background petal and anther was larger than 0.2 hex units for both types of anthers whereby honeybees can detect. The pairwise distance between the loci of two types of anthers was less than 0.1 hex units, indicating that honeybees cannot distinguish them by reflectance. The sterile pollen emits blue fluorescence in addition to the reflectance (fluoresced+reflected photons), enhancing the visual signaling to pollinators. Since honeybees prefer the blue fluorescence of **1** (Mori et al. 2018), the fluorescence may have an influence on their foraging behavior.

One possible cause of the low and fluctuating yield of *P. mume* is abnormal sterile pollen, likely induced by low-temperature stress during male reproductive development. Another cause is the foraging efficiency of honeybees introduced into orchards (Nakanishi 1982). The sterile pollen was devoid of starch granules and so may be less nutritious for honeybees compared to the fertile pollen. However, if pollinating honeybees preferred to visit flowers with sterile pollen, the cross-pollination efficiency of *P. mume* might deteriorate.

Acknowledgements

We thank Ryutaro Tao, Hisayo Yamane, and Takashi Akagi (Graduate School of Agriculture, Kyoto University); Yuto Kitamura (Japanese Apricot Research Laboratory, Wakayama Research Center) for valuable discussion on the pollen development; Mizuho Hanaki (Graduate School of Agriculture, Kyoto University) and Katsutoshi Nishino (Graduate School of Biostudies, Kyoto University) for the mass spectral measurements; Tetsuhito Suzuki (Graduate School of Agriculture, Kyoto University) for the diffuse reflectance spectral measurements; and Keiko Okamoto-Furuta and Haruyasu Kohda (Center for Anatomical, Pathological and Forensic Medical Researches, Graduate School of Medicine, Kyoto University) for their technical assistance with electron microscopy. This work was supported in part by MEXT KAKENHI (grant Numbers 16H06470, 16H06464, 16K21727 to MW), JSPS KAKENHI (grant Numbers 17H00821, 18KT0048, 19K22342 to MW) and JSPS Bilateral Programs (grant Number 18032211-000481 to MW).

References

Alcázar R, Altabella T, Marco F, Bortolotti C, Reymond M, Koncz C, Carrasco P, Tiburcio AF (2010) Polyamines: Molecules with regulatory functions in plant abiotic stress tolerance. *Planta* 231: 1237–1249

Anwar R, Matoo A, Handa AK (2015) Polyamine interactions with plant hormones: Crosstalk at several levels. In: Kusano T, Suzuki H (eds) *Polyamines: A universal molecular nexus for growth, survival, and specialized metabolism*. Springer, New York, pp 267–302

Bassard JE, Ullmann P, Bernier F, Werck-Reichhart D (2010) Phenolamides: Bridging polyamines to the phenolic metabolism. *Phytochemistry* 71: 1808–1824

Bennini B, Chulia AJ, Kaouadji M, Thomasson F (1992) Flavonoid glycosides from *Erica cinerea*. *Phytochemistry* 31: 2483–2486

Birkofer L, Kaiser C, Nouvertné W, Thomas U (1961) Natürlich vorkommende Zuckerester von Phenolcarbonsäuren. *Z Naturforsch B* 16: 249–251

Bitrián M, Zarza X, Altabella T, Tiburcio AF, Alcázar R (2012) Polyamines under abiotic stress: Metabolic crossroads and hormonal crosstalks in plants. *Metabolites* 2: 516–528

Bokern M, Witte L, Wray V, Nimtz M, Meurer-Grimes B (1995) Trisubstituted hydroxycinnamic acid spermidines from *Quercus dentata* pollen. *Phytochemistry* 39: 1371–1375

Bokern M, Wray V, Strack D (1987) Hydroxycinnamic acid esters of glucuronosylglucose from cell suspension cultures of

Chenopodium rubrum. *Phytochemistry* 26: 3229–3231
Bowmaker JK, Dartnall HJA (1980) Visual pigments of rods and cones in a human retina. *J Physiol* 298: 501–511
Burgos L, Alburquerque N, Egea J (2004) Review. Flower biology in apricot and its implications for breeding. *Span J Agric Res* 2: 227–241
Carrizo García C, Nepi M, Pacini E (2017) It is a matter of timing: Asynchrony during pollen development and its consequences on pollen performance in angiosperms-a review. *Protoplasma* 254: 57–73
Chittka L (1992) The colour hexagon: A chromaticity diagram based on photoreceptor excitations as a generalized representation of colour opponency. *J Comp Physiol A* 170: 533–543
Chittka L, Beier W, Hertel H, Steinmann E, Menzel R (1992) Opponent colour coding is a universal strategy to evaluate the photoreceptor inputs in Hymenoptera. *J Comp Physiol A* 170: 545–563
Chittka L, Vorobyev M, Shmida A, Menzel R (1993) Bee colour vision-The optimal system for the discrimination of flower colours with three spectral photoreceptor types? In: Wiese K, Gribakin FG, Popov AV, Renninger G (eds) *Sensory Systems of Arthropods*. Birkhäuser, Basel, pp 211–218
Dixon RA, Paiva NL (1995) Stress-induced phenylpropanoid metabolism. *Plant Cell* 7: 1085–1097
Elejalde-Palmett C, de Bernonville TD, Glevarec G, Pichon O, Papon N, Courdavault V, St-Pierre B, Giglioli-Guivarc'h N, Lanoue A, Besseau S (2015) Characterization of a spermidine hydroxycinnamoyltransferase in *Malus domestica* highlights the evolutionary conservation of trihydroxycinnamoyl spermidines in pollen coat of core Eudicotyledons. *J Exp Bot* 66: 7271–7285
Ferreres F, Tomás-Barberán FA, Tomás-Lorente F, Nieto JL, Rumbero A, Olías JM (1989) 8-Methoxykaempferol 3-sophoroside, a yellow pigment from almond pollen. *Phytochemistry* 28: 1901–1903
Grienenberger E, Besseau S, Geoffroy P, Debayle D, Heintz D, Lapierre C, Pollet B, Heitz T, Legrand M (2009) A BAHD acyltransferase is expressed in the tapetum of Arabidopsis anthers and is involved in the synthesis of hydroxycinnamoyl spermidines. *Plant J* 58: 246–259
Hayashi K, Shimazu K, Yaegaki H, Yamaguchi M, Iketani H, Yamamoto T (2008) Genetic diversity in fruiting and flower-ornamental Japanese apricot (*Prunus mume*) germplasms assessed by SSR markers. *Breed Sci* 58: 401–410
Hixson JL, Hayasaka Y, Curtin CD, Sefton MA, Taylor DK (2016) Hydroxycinnamoyl glucose and tartrate esters and their role in the formation of ethylphenols in wine. *J Agric Food Chem* 64: 9401–9411
Hou JH, Gao ZH, Zhang Z, Chen SM, Ando T, Zhang JY, Wang XW (2011) Isolation and characterization of an *AGAMOUS* homologue *PmAG* from the Japanese apricot (*Prunus mume* Sieb. et Zucc.). *Plant Mol Biol Report* 29: 473–480
Jiang J, Zhang Z, Cao J (2013) Pollen wall development: The associated enzymes and metabolic pathways. *Plant Biol* 15: 249–263
Jiang JS, Lü L, Yang YJ, Zhang JL, Zhang PC (2008) New spermidines from the flowers of *Carthamus tinctorius*. *J Asian Nat Prod Res* 10: 447–451
Johansen DA (1940) *Plant Microtechnique*. McGraw-Hill Publications, New York
Koeppe DE, Rohrbaugh LM, Rice EL, Wender SH (1970) The effect of age and chilling temperatures on the concentration of scopolin and caffeoylquinic acids in tobacco. *Physiol Plant* 23: 258–266
Liu T, Kim DW, Niitsu M, Maeda S, Watanabe M, Kamio Y, Berberich T, Kusano T (2014) Polyamine oxidase 7 is a terminal catabolism-type enzyme in *Oryza sativa* and is specifically expressed in anthers. *Plant Cell Physiol* 55: 1110–1122
Mackenzie G, Boa AN, Diego-Taboada A, Atkin SL, Sathyapalan T (2015) Sporopollenin, the least known yet toughest natural biopolymer. *Front Mater* 2: 66
Maia R, Eliason CM, Bitton PP, Doucet SM, Shawkey MD (2013) Pavo: An R package for the analysis, visualization and organization of spectral data. *Methods Ecol Evol* 4: 906–913
Mamun EA, Alfred S, Cantrill LC, Overall RL, Sutton BG (2006) Effects of chilling on male gametophyte development in rice. *Cell Biol Int* 30: 583–591
Mamun EA, Cantrill LC, Overall RL, Sutton BG (2010) Mechanism of low-temperature-induced pollen failure in rice. *Cell Biol Int* 34: 469–476
Martin-Tanguy J (2001) Metabolism and function of polyamines in plants: Recent development (new approaches). *Plant Growth Regul* 34: 135–148
Matsuno M, Compagnon V, Schoch GA, Schmitt M, Debayle D, Bassard JE, Pollet B, Hehn A, Heintz D, Ullmann P, et al. (2009) Evolution of a novel phenolic pathway for pollen development. *Science* 325: 1688–1692
Ministry of Agriculture, Forestry and Fisheries (2018) Statistical yearbook of Ministry of Agriculture, Forestry and Fisheries. http://www.maff.go.jp/e/data/stat/nenji_index.htm. Accessed 29 March 2021
Morant M, Schoch GA, Ullmann P, Ertunç T, Little D, Olsen CE, Petersen M, Negrel J, Werck-Reichhart D (2007) Catalytic activity, duplication and evolution of the CYP98 cytochrome P450 family in wheat. *Plant Mol Biol* 63: 1–19
Mori S, Akamatsu M, Fukui H, Tsukioka J, Goto K, Hirai N (2019) The unusual conformational preference of N^1,N^5,N^{10}-tri-*p*-coumaroylspermidine *E-Z* isomers from the Japanese apricot tree, *Prunus mume*, for the (*ZZZ*)-form. *Phytochem Lett* 31: 131–139
Mori S, Fukui H, Oishi M, Sakuma M, Kawakami M, Tsukioka J, Goto K, Hirai N (2018) Biocommunication between plants and pollinating insects through fluorescence of pollen and anthers. *J Chem Ecol* 44: 591–600
Moschou PN, Wu J, Cona A, Tavladoraki R, Angelini R, Roubelakis-Angelakis A (2012) The polyamines and their catabolic products are significant players in the turnover of nitrogenous molecules in plants. *J Exp Bot* 63: 5003–5015
Nakanishi T (1982) Morphological and ultraviolet absorption differences between fertile and sterile anthers of Japanese apricot cultivars in relation to their pollination stimuli. *Sci Hortic* 18: 57–63
Nakanishi T, Ichii T (1978) The factors affecting fruit set in pollenless variety of Japanese apricot. III. The frequencies of insects visiting flowers and fruit set. *Science Report of Faculty of Agriculture. Kobe University* 13: 75–80
Oda S, Kaneko F, Yano K, Fujioka T, Masuko H, Park J-I, Kikuchi S, Hamada K, Endo M, Nagano K, et al. (2010) Morphological and gene expression analysis under cool temperature conditions in rice anther development. *Genes Genet Syst* 85: 107–120
Osaka M, Matsuda T, Sakazono S, Masuko-Suzuki H, Maeda S, Sewaki M, Sone M, Takahashi H, Nakazono M, Iwano M, et al. (2013) Cell type-specific transcriptome of Brassicaceae stigmatic papilla cells from a combination of laser microdissection and RNA sequencing. *Plant Cell Physiol* 54: 1894–1906
Parker CA, Rees WT (1962) Fluorescence spectrometry. A review. *Analyst* 87: 83–111

Peitsch D, Fietz A, Hertel H, de Souza J, Ventura DF, Menzel R (1992) The spectral input systems of hymenopteran insects and their receptor-based colour vision. *J Comp Physiol A* 170: 23–40

Perkin AG (1909) CCXXXIV.-The colouring matter of cotton flowers. *Gossypium herbaceum*. part II. *J Chem Soc Trans* 95: 2181–2193

Potts SG, Imperatriz-Fonseca V, Ngo HT, Aizen MA, Biesmeijer JC, Breeze TD, Dicks LV, Garibaldi LA, Hill R, Settele J, et al. (2016) Safeguarding pollinators and their values to human well-being. *Nature* 540: 220–229

Punt W, Hoen PP, Blackmore S, Nilsson S, Le Thomas A (2007) Glossary of pollen and spore terminology. *Rev Palaeobot Palynol* 143: 1–81

Quilichini TD, Grienenberger E, Douglas CJ (2015) The biosynthesis, composition and assembly of the outer pollen wall: A tough case to crack. *Phytochemistry* 113: 170–182

R Core Team (2016) R: A language and environment for statistical computing. Vienna, Austria: R Foundation for statistical computing. https://www.R-project.org/

Rozema J, Broekman RA, Blokkerb P, Meijkampa BB, de Bakkera N, van de Staaij J, van Beem A, Ariese F, Kars SM (2001) UV-B absorbance and UV-B absorbing compounds (*para*-coumaric acid) in pollen and sporopollenin: The perspective to track historic UV-B levels. *J Photochem Photobiol B* 62: 108–117

Sanders PM, Bui AQ, Weterings K, McIntire KN, Hsu YC, Lee PY, Truong MT, Beals TP, Goldberg RB (1999) Anther developmental defects in *Arabidopsis thaliana* male-sterile mutants. *Sex Plant Reprod* 11: 297–322

Sharma KD, Nayyar H (2016) Regulatory networks in pollen development under cold stress. *Front Plant Sci* 7: 402

Sobolev VS, Sy AA, Gloer JB (2008) Spermidine and flavonoid conjugates from peanut (*Arachis hypogaea*) flowers. *J Agric Food Chem* 56: 2960–2969

Song JH, Moon H-K, Hong S-P (2016) Pollen morphology of the tribe Sorbarieae (Rosaceae). *Plant Syst Evol* 302: 853–869

Song JH, Oak M-K, Roh H-S, Hong S-P (2017) Morphology of pollen and orbicles in the tribe Spiraeeae (Rosaceae) and its systematic implications. *Grana* 56: 351–367

Sun H, Shi T, Song J, Xu Y, Gao Z, Song X, Ni Z, Cai B (2016) Pistil abortion in Japanese apricot (*Prunus mume* Sieb. et Zucc.): Isolation and functional analysis of *PmCCoAOMT* gene. *Acta Physiol Plant* 38: 114

Tao R, Habu T, Namba A, Yamane H, Fuyuhiro F, Iwamoto K, Sugiura S (2002) Inheritance of S^f-RNase in Japanese apricot (*Prunus mume*) and its relation to self-compatibility. *Theor Appl Genet* 105: 222–228

Vogt T (2010) Phenylpropanoid biosynthesis. *Mol Plant* 3: 2–20

Watanabe M, Shiozawa H, Isogai A, Suzuki A, Takeuchi T, Hinata K (1991) Existence of S-glycoprotein-like proteins in anthers of self-incompatible species of *Brassica*. *Plant Cell Physiol* 32: 1039–1047

Werner C, Hu W, Lorenzi-Riatsch A, Hesse M (1995) Di-coumaroylspermidines and tri-coumaroylspermidines in anthers of different species of the genus *Aphelandra*. *Phytochemistry* 40: 461–465

Wimalasekera R, Tebartz F, Scherer GFE (2011) Polyamines, polyamine oxidases and nitric oxide in development, abiotic and biotic stresses. *Plant Sci* 181: 593–603

Xu D, Shi J, Rautengarten C, Yang L, Qian X, Uzair M, Zhu L, Luo Q, An G, Waßmann F, et al. (2017) Defective Pollen Wall 2 (DPW2) encodes an acyl transferase required for rice pollen development. *Plant Physiol* 173: 240–255

Yaegaki H, Miyake M, Haji T, Yamaguchi M (2003) Inheritance of male sterility in Japanese apricot (*Prunus mume*). *HortScience* 38: 1422–1423

Yu Z, Jia D, Liu T (2019) Polyamine oxidases play various roles in plant development and abiotic stress tolerance. *Plants* 8: 184

Zhao G, Qin GW, Gai Y, Guo LH (2010) Structural identification of a new tri-*p*-coumaroylspermidine with serotonin transporter inhibition from safflower. *Chem Pharm Bull* 58: 950–952

Zinn KE, Tunc-Ozdemir M, Harper JF (2010) Temperature stress and plant sexual reproduction: Uncovering the weakest links. *J Exp Bot* 61: 1959–1968